Arabian Journal of Chemistry (2021) **14**, 102921

King Saud University

Arabian Journal of Chemistry

www.ksu.edu.sa
www.sciencedirect.com

ORIGINAL ARTICLE

Two new coordination polymers: Magnetic properties and treatment activity on non-small cell lung cancer by reversing the resistance of the cancer cells

Yi-Long Wan [a,1], Yun-Yun Xu [b,1], Bo Peng [a], Ling-Di Zhao [c], Quan-Li Gao [c], Dong Jiang [a,*]

[a] *Department of Thoracic Surgery, The First Affiliated Hospital of Soochow University, Suzhou, Jiangsu, China*
[b] *Institute of Pediatrics, Childrens' Hospital Affiliated to Soochow University, Suzhou, Jiangsu, China*
[c] *Department of Medicine, Zhengzhou University, Zhengzhou, Henan, China*

Received 26 September 2020; revised 19 November 2020; accepted 29 November 2020
Available online 3 December 2020

KEYWORDS

Coordination complexes;
Magnetic properties;
NSCLC;
RT-PCR

Abstract In the current study, by employing 5-((4-carboxypyridin-2-yl)amino)isophthalic acid (H_3L) as semirigid carboxylate-pyridine ligand with V-shape, two new transition metal coordination polymers with the chemical formulae of $[Cu_{1.5}(L)(H_2O)]\cdot 2H_2O$ (**1**) and $[Co_4(L)_2(CH_3CN)(OH)_2(H_2O)_4]\cdot 3H_2O$ (**2**) have been successfully prepared through the reaction between the H_3L ligand and corresponding metal salts under the solvothermal reaction conditions. Magnetic investigations have suggested that there is antiferromagnetic coupling between neighboring metal ions in the two compounds. The application values of compounds **1** and **2** on the non-small cell lung cancer (NSCLC) was evaluated and the related mechanism was discussed at the same time. First of all, the Cell Counting Kit-8 (CCK-8) detection kit was performed to measure the viability of the non-small cell lung cancer cells after compound treatment. In addition to this, the real time reverse transcription polymerase chain reaction (real time RT-PCR) was used to detect the relative expression levels of the *ezh2* gene in NSCLC cells after indicated treatment.

1. Introduction

Lung cancer is my country's number one cancer killer. Among the 653,000 new lung cancer patients in my country each year, non-small cell lung cancer (NSCLC) patients account for 85%. Since the appearance of targeted drugs, lung cancer patients have inevitably developed drug resistance and disease progression over time, and there is an urgent need for new drugs to

* Corresponding author.
E-mail address: okivvlja7053@163.com (D. Jiang).

[1] Authors are contributed equally to this work.

Peer review under responsibility of King Saud University.

ELSEVIER Production and hosting by Elsevier

https://doi.org/10.1016/j.arabjc.2020.102921

prolong life of NSCLC patients (Rodriguez-Canales et al., 2016; Romaszko and Doboszyńska, 2018). In 2011, the incidence of lung cancer in my country was 48.32 per 100,000, and the mortality rate was 39.27 per 100,000. The incidence and mortality of lung cancer ranked first among malignant tumors (de Sousa and Carvalho, 2018). Chemotherapy is the main treatment for advanced NSCLC. Although its status has not changed fundamentally, its efficacy has reached a plateau. At the same time, the side effects of chemotherapy have also restricted its wide clinical application (Mao et al., 2016). Thus, in this research, new candidates for the NSCLC treatment was developed.

In the field of functional materials, coordination polymers (CPs) are the active study topic, which have obtained great attention, this is owing to their diversity of composition and the distinctive abilities of structural tailoring, this also due to their applications in electrochemical sensing, luminescence, adsorption separation and other fields (Coudert and Fuchs, 2015; Jiang et al., 2020; He et al., 2020; Zhao et al., 2021; Karmakar et al., 2016) The diversity of their performances and structures depends on the diversity of assembly approaches and the number of components, which is directly associated with the components coordination characteristics, for instance, the dentates number, charge, types and position of substituents, as well as the ligands steric hindrance (Duan et al., 2020; Rancan and Armelao, 2015; Liu et al., 2014; Zheng et al., 2019; Bai et al., 2018). Currently, CPs established with the rigid aromatic polycarboxylic acid ligands, for example, a variety of positional isomer pyridine dicarboxylate ligands and modified terephthalic acid ligands, have been reported frequently; nevertheless, there are few studies on the establishment of CPs utilizing the semi-rigid nitrogen-heterocyclic carboxylic acid ligands; because N atom and O atom possess strong coordination ability with a variety of transition ions, semi-rigid nitrogen-heterocyclic carboxylic acid ligands are the ideal choice to establish the functional CPs containing rich hydrogen-bond interaction positions and strong skeleton stability (Zhao et al., 2021; Chen et al., 2016; Yang et al., 2020; Han et al., 2015; Sen et al., 2020; Mukherjee et al., 2018). In this study, by employing 5-((4-carboxypyridin-2-yl)amino)isophthalic acid (H_3L), a semi-rigid carboxylate-pyridine ligand with V-shape, two new transition metal coordination polymers with the chemical formulae of $[Cu_{1.5}(L)(H_2O)\cdot 2H_2O$ (**1**) and $[Co_4(L)_2(CH_3CN)(OH)_2(H_2O)_4]\cdot 3H_2O$ (**2**) have been successfully prepared through the reaction between the H_3L ligand and corresponding metal salts under the solvothermal reaction conditions. The as-synthesized two polymers were completely explored with PXRD, TGA, the diffraction of single crystal X-ray, IR spectroscopy as well as EA. Magnetic investigations have suggested that there is antiferromagnetic coupling between neighboring metal ions in the two compounds. Their treatment activity against the NSCLC was assessed and the detail mechanism was discussed as well. The results of the CCK-8 assay indicated that compound **1** was more excellent than compound **2** on inhibiting the viability of the NSCLC cells. Besides, the data of the real time RT-PCR revealed that compound **1** could significantly inhibit the relative expression of the *ezh2* gene in the NSCLC cells, but compound **2** exhibited only little change on the *ezh2* gene expression.

2. Experimental

2.1. Chemicals and measurements

The solvents and reagents utilized in our work could be gained from market, which could be utilized with no in-depth purification. For the compounds' infrared spectra utilizing KBr pellets (with 5 mg sample in the 500 mg KBr), it was implemented with the FT-IR spectrometer of Nicolet (Impact 410), with 400–4000 cm^{-1} infrared spectra range. By utilizing the Elemental analyzer of Perkin–Elmer 240C, we analyzed the elements of Hydrogen, Nitrogen and Carbon. For the determinations of PXRD, we can implement it through applying the Cu Kα radiation (with λ of 1.5418 Å) X-ray diffractometer of Bruker D8 Advance, where the X-ray tube worked at 40 mA and 40 kV. The as-prepared samples were characterized with the TGA in the atmosphere of N_2 at 10 K min^{-1} heating rate on the thermogravimetric analyzer of Perkin-Elmer Pyris 1 TGA up to 1023 K, and the measurement of magnetic performances was carried out with the PPMS-9 ACMS magnetometer and the Quantum Design MPMS-XL7. The antimagnetic corrections to all constituent atoms were carried out via applying the Pascal's constants.

2.2. Preparation and characterization for $[Cu_{1.5}(L)(H_2O)]\cdot H_2O$ (1) and $[Co_4(L)_2(CH_3CN)(OH)_2(H_2O)_4]\cdot 3H_2O$ (2)

We stored the mixture of 25.0 mg and 0.1 mmol $CuSO_4\cdot 5H_2O$, 15.2 mg and 0.05 mmol H_3L, 4 mL of H_2O and 4 mL of CH_3CN into the 15 mL stainless steel container with Teflon lining, and that, the mixture is first heated for three days under the temperature of 120 °C, and then it was cooled to the indoor ambient temperature with the 10 °C·h^{-1} rate. After accomplishing the above steps, we can gain the massive blue crystals, which possesses 36.6% yield. Elemental analysis, calculated (%) (**1**): N 3.08%, H 2.86%, and C 39.60%; found: N 3.21%, H 2.63%, and C 39.52%. FTIR: 485 (w), 607 (w), 736 (w), 779 (w), 989 (w), 1110 (m), 1251 (w), 1396 (s), 1562 (m), 1625 (m), 3480 (s), 3573 (m).

Subsequently, we stored the mixture of 28.1 mg and 0.1 mmol $CoSO_4\cdot 7H_2O$, 15.2 mg and 0.05 mmol H_3L, 4 mL of H_2O and 4 mL of CH_3CN as well as three drops of 1 mol L^{-1} NaOH into the 15 mL stainless steel container with Teflon lining, after that, the mixture is first heated for three days under the temperature of 150°C, and then it was cooled to the indoor ambient temperature with the 10 °C·h^{-1} rate. After accomplishing all the above steps, we can gain the massive red crystals, which possesses 57.2% yield. Elemental analysis, calculated (%) (**2**): N 5.33%, H 1.71%, and C 31.96%; found: N 5.24%, H 1.95%, and C 31.87%. FTIR (KBr, cm^{-1}): 503 (w), 555 (w), 711 (w), 775 (w), 993 (w), 1124 (w), 1238 (w), 1386 (s), 1579 (s), 1625 (s), 3305 (m), 3552 (m).

The diffractometer of SuperNova was applied to acquire the data of X-ray. The analysis of strength data was conducted with the software of CrysAlisPro and then it can be converted to the files of HKL. The original structural patterns were established via the direct method based program of SHELXS, and the least-squares means based program of SHELXL-2014 was modified. With the overall non-H atoms, the anisotropic parameters could be mixed. Later, the overall hydrogen atoms were fixed on carbon atoms geometrically that they are con-

nected to via applying the commands of AFIX. The two complexes's parameters of crystallography and their refinement details were summed up in Table 1 in detail. The selected bond lengths and angles are shown in the Tables S1–S4 in the ESI file.

2.3. Cell Counting Kit-8

After treated with compounds **1** and **2**, the viability of the NSCLC cells was determined with Cell Counting Kit-8 detection kit. This preformation was conducted totally under the guidance of the instructions with only a little modification. In brief, the A549 NSCLC cells in the logical growth phage were harvested and seeded into the 96 well plates at the final destiny of 10^5 cells per well. Subsequently, the culture plates were placed in an incubatory at the condition of 5% CO_2 and 37 °C for 12 h. When the cell step into the confluence of 75%, the compound was added into the wells at the serial diluted concentration for incubation. After that, the cell culture medium was discarded and the fresh medium containing CCK-8 reagent was applied, and then the cells were cultured for another four hours. Finally, the microplate reader was utilized for the determination of the absorbance at 450 nm in each well.

2.4. Real time RT-PCR

The real time RT-PCR was then carried out in this present research to evaluate the relative expression levels of the *ezh2* gene in the A549 NSCLC cells. This experiment was finish[ed] strictly in accordance with the instructions with some change. In short, the A549 NSCLC cells in logical growth phage were harvested and inoculated into 6 well culture pla[tes] (1[0] cells/well). After that, the culture plates were kept [in] the inc[ubator] at the condition of 5% CO_2 and 37 °C for [1] d[ay]. Afterwards, compounds **1** and **2** was add[ed] into [the] wells at 5 mg/kg concentration for the indica[ted] treatmen[t]. Next, the A549 NSCLC cells were collected [and] the total RN[A] in the cancer cells was extracted with TRIZOL r[eagent]. The concentration of the total RNA wa[s] measured and [then] reverse transcripted into cDNA accor[ding] to the protocols. The *ezh2* gene relative expression in t[he] A549 N[SCLC] cells was detected via the real time reverse tran[scription] polym[erase] chain reaction, with *gapdh* used [as] control gene.

3. Results and discussion

3.1. Crystal structures

From the results of single-crystal X-ray, it can be seen that complex **1** was crystallized in a monoclinic *C*2/*c* space group, which displays a three-dimensional microporous skeleton. The **1**'s asymmetric unit includes a coordinated molecule of water, a completely deprotonated ligand of L^{3-} as well as 1.5 ions of Cu(ii). In the Fig. 1a, the Cu1 ion is coordinated with two nitrogen and two oxygen atoms in four ligands of L^{3-}, thereby producing a distorted geometry of square. While the Cu2 ion is coordinated with a molecule of water and five oxygen atoms originate from four ligands of L^{3-} in order to generate a coordinate geometry of square pyramid, where

Table 1 The two complexes's parameters of crystallography and their refinement details.

Identification code	**1**	**2**
Empirical formula	$C_{28}H_{18}Cu_3N_4O_{14}$	$C_{30}H_{33}Co_4N_5O_{22}$
Formula weight	825.11	1051.33
Temperature/K	124.3(5)	298.15
Crystal system	monoclinic	triclinic
Space group	C2/c	P-1
a/Å	14.552(4)	8.13620(10)
b/Å	13.0230(10)	11.0570(2)
c/Å	24.036(2)	11.2690(3)
α/°	90	98.9260(10)
β/°	97.159(3)	97.475(2)
γ/°	90	[1]2.063(2)
Volume/Å^3	4519.6(13)	9[0]1(3)
Z	4	1
ρ_{calc}g/cm^3	1.213	1.922
μ/mm^{-1}	1.45[1]	1.896
Data/ restraints/parameters	4[1]0/35/231	33[8]/18/293
Goodness-of-fit on F^2	[1].074	1.048
Final R indexes [I > = 2σ (I)]	R[1] = 0.0369, ωR$_2$ = 0.10[9]	R$_1$ = 0.0268, ωR$_2$ = 0.0734
Final R indexes [all data]	R$_1$ = 0.[0]5[6], ωR$_2$ = 0.1104	R$_1$ = 0.0280, ωR$_2$ = 0.0743
Largest diff. peak/hole/e Å^{-3}	[0].59/−0.66	0.86/−0.94
CCDC	2,034,036	2,034,037

equator[ial] [pl]ane was took up by four carboxylic acid oxygen atoms, and the short distances of Cu–O is between 1.943(2)Å and 1.9[7]1(2) Å, while a water oxygen atom lies in axis apex, and the relatively longer length of bond is 2.139(2) Å. The bridging bidentate ($\eta^2\mu_2\chi^2$) and monodentate ($\eta^1\mu_1\chi^1$) manners of carboxylic acid groups in the ligand of L^{3-} consists in complex **1**, and generated a paddlewheel SBU of $[Cu_2(COO)_4]$ (Fig. 1b). With the calculation of the distance between adjacent carbon atoms in two lateral connectors of L^{3-}, the SBUs were in-depth extended through the L^{3-} connectors to produce the three-dimensional porous skeleton containing one-dimensional channels with an opening of 11.10 × 8.86 Å^2 (Fig. 1c). The lattice molecules of H_2O occupied the channels. After calculating, the volume of void accounts for 47.7% of the overall crystal volume. In complex **1**, a linkers of L^{3-} is linked to two centers of Cu1 and two SBUs of $[Cu_2(COO)_4]$ can be regarded as a 4-linked node. Furthermore, both the centers of Cu1 and the SBUs of $[Cu_2(COO)_4]$ can be reduced as 4-linked nodes. Hence, the trinodal (4,4,4)-linked novel topological network with $(4{\cdot}6^5)_2(4^2{\cdot}6^2{\cdot}8^2)(6^4{\cdot}8^2)$ point symbol was produced by complex **1** (Fig. 1d).

For complex **2**, it was crystallized in a triclinic $P-1$ space group. And its asymmetric unit is accomplished by two completely deprotonated ligands of L^{3-}, four separate Co(ii) ions, a coordinated molecule of acetonitrile, four coordinated molecules of water as well as two hydroxyls. From the resultsr exhibited in Fig. 2a, the Co1 ion is coordinated with a molecule of acetonitrile, two hydroxyls oxygen atoms and five oxygen atoms with three oxygen atoms in three ligands of L^{3-}. while the Co2 ion is coordinated with six oxygen atoms come from four ligands of L^{3-} and two molecules of water, thereby generating a distorted geometry of octahedron. It can be seen

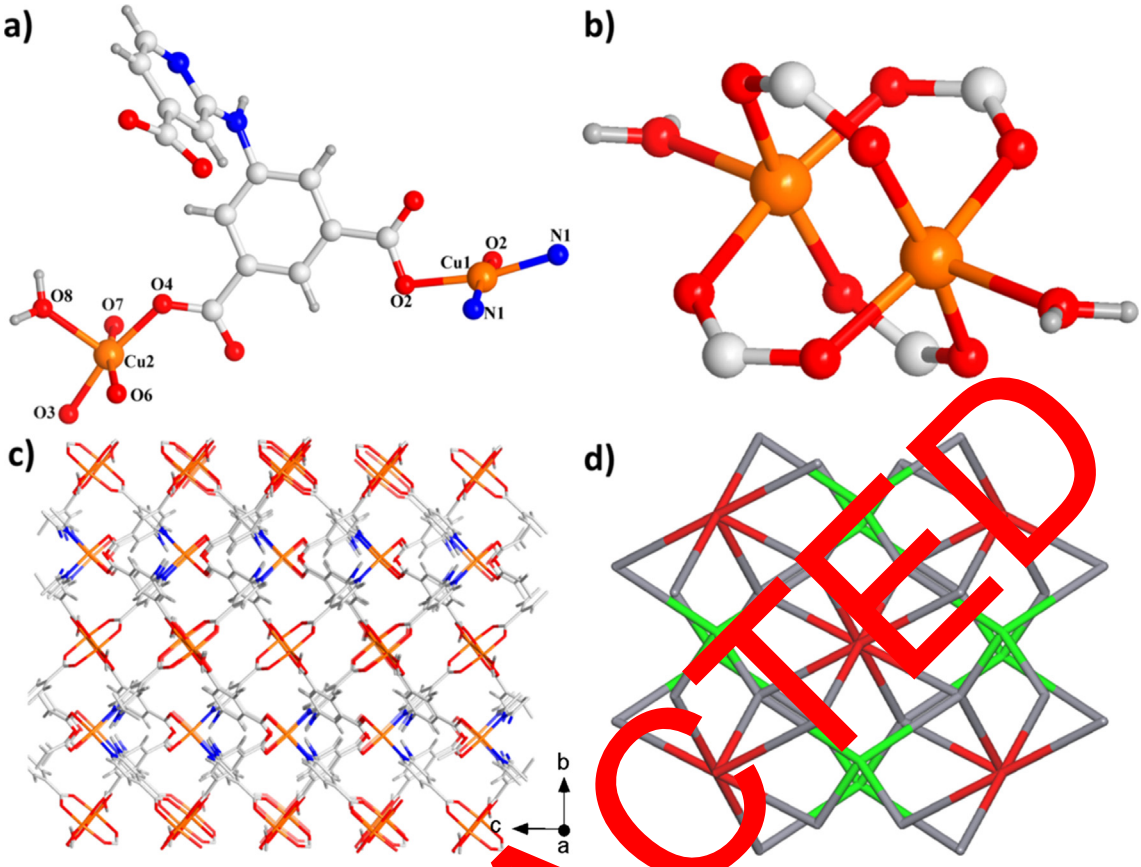

Fig. 1 (a) The diagram for the **1**'s asymmetry unit. (b) The paddlewheel SBU of $[Cu_2(COO)_4]$. (c) The three-dimensional skeleton of **1**. (d) The **1**'s 3-nodal (4,4,4)-linked network.

that the length of Co—N bond is 2.136 Å and that of Co—O bonds is between 2.030 Å and 2.245 Å. In complex **2**, the three carboxylic acids in ligand L^{3-} are coordinated with six Co(ii) ions, which utilizes two dissimilar coordination manners, namely, bridging monodentate ($\eta^1\mu^2\chi^1$) and bridging bidentate ($\eta^2\mu^2\chi^2$). In addition, two Co2 ions and two Co1 ions were linked via two hydroxyl and six carboxylic acid groups for the formation of the tetranuclear SBU of $[Co_4(COO)_6(\mu_3\text{-}OH)_2]$, in which the separation of Co···Co is varying from 3.1220 (4) Å to 3.5235 Å (Fig. 2b). This kind of cluster is rarely appeared in the complexes, which is similar to that in the $\{[Co_4(OH)_2(p\text{-cbia})_2(bpmp)(H_2O)_3]\cdot 2H_2O\}_n$. Furthermore, in complex **2**, SBU is extended via six ligands L^{3-} in order to form the two-dimensional layer (Fig. 2c). In topology, the SBU of $[Co_4(COO)_6(\mu_3\text{-}OH)_2]$ and L^{3-} ligand can respectively be regarded as 6-linked and 3-linked nodes; therefore, **2** reflected a (3,6)-linked network with ***kgd*** topology, where the point symbol is $(4^3)_2(4^6{\cdot}6^6{\cdot}8^3)$ (Fig. 2d).

For the sake of the detection of products' phase purity, we conducted the investigation of powder X-ray diffraction on our prepared complexes (Fig. 3a). The peak position of simulated PXRD pattern is in consistent with that of the experiment, which suggests that the crystal architecture really represents the products of bulk crystal. The selective selection of crystal samples will result in the difference of product strength. For the two compounds, the determinations of TGA was performed for the detection of their thermal stabilities. The weightlessness htlessness rate of complex **1** is 12.4% in the temperature range of ambient temperature to 97 °C, which is in accordance with the removal of disordered lattice molecules of solvent and coordination H_2O (with the calculated value of 12.9%). In 97–255 °C temperature, its structure is still relatively stable, then the structure started to collapse rapidly. The weightlessness rate of complex **2** was 16.4% (with the calculated value of 17.3%) when the temperature was lower than 158 °C, which equivalent to the release of water molecules and coordination acetonitrile and the lattice molecules of water.

3.2. Magnetic properties

At the 2 K to 300 K temperature, and 1000 Oe dc magnetic field, these compounds' viable-temperature magnetic susceptibilities have been explored. From structure analysis, each L^{2-} ligand coordinated with two paddlewheel Cu(II) ions to produce a 3D framework. The distance between the adjacent paddlewheel SBUs is 9.764 Å. Therefore, when discuss the magnetic properties of **1**, **1** can be viewed as the two unclear SBUs. As shown in Fig. 4, the value of $\chi_M T$ at ambient temperature is 1.86 cm^3 K mol^{-1}, this value is greater than the pure spin value for three Cu(II) ions 1.125 cm^3 K mol^{-1} ($g = 2$ and $S = 1/2$)(Cui et al., 2019). The value of χ_MT decreased steadily to the minimum value 0.84 cm^3 K mol^{-1} when the temperature cooled to 2 K, which shows the antifer-

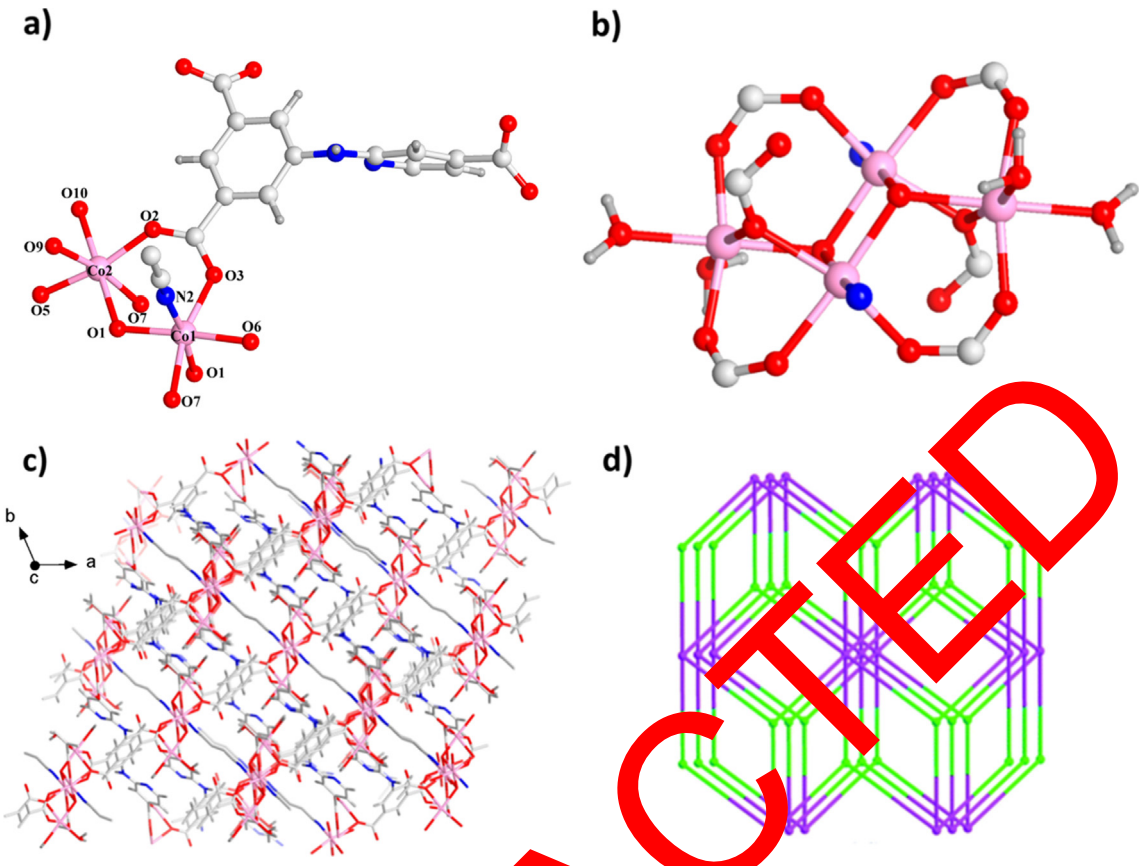

Fig. 2 (a) The diagram for the **1**'s asymmetry unit. (b) The S[illegible] of [illegible](COO)$_6$(μ_3-OH)$_2$] for complex **2**. (c) The **1**'s three-dimensional skeleton reflecting the one-dimensional channels. (d) The (3,6)-li[illegible]ked [illegible]with ***kgd*** topology of **2**.

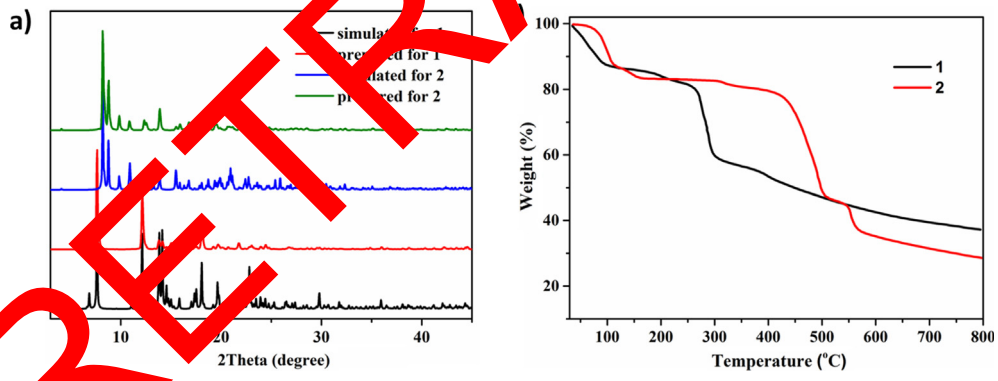

Fig. 3 (a) The PXRD patterns for **1** and **2**. (b) The TGA curves for **1** and **2**.

romagnetic properties in **1**. And further, the reciprocal susceptibility $1/\chi_m$ in 25–300 K fit Curie–Weiss law $\chi_M = C/(T - \theta)$, giving θ = -7.88 K and C = 2 cm^3 K mol^{-1}. The negative constant of Weiss θ reflects that there is an antiferromagnetic interaction between the Cu (II) ions in **1** (Zhang et al., 2020).

These compounds' variable-temperature magnetic susceptibilities detected, and illustrated as the χ_M^{-1} and χ_MT versus T plots (Fig. 5). At 300 K, measured value of χ_MT is 11.3 cm^3 K mol^{-1}, which is greater than the expected high spin-only 7.5 cm^3 K mol^{-1} for five magnetically isolated Co(II) ions [S = 3/2, g = 2, 1.875 cm^3 K mol^{-1} for one Co(II)], which may be caused by the large contribution of the residual orbitals (Yang et al., 2011; Yao et al., 2013). When the temperature drops to 50 K, the χ_MT value decreased slowly. And the value of χ_MT declines sharply to the minimum value 1.9 cm^3 K mol^{-1} at 2 K. This result reveals that there exists an antiferromagnetic coupling in complex **2**. The temperature dependence of the reciprocal susceptibilities (χ_M^{-1}) from 10 K to 300 K follows the law of Curie–Weiss: $\chi_M = C/(T - \theta)$, where the Curie constant of C is 12.5 cm^3 K mol^{-1} and the Weiss constant of θ is − 30.5 K. The negative value of θ shows that there is exists the antiferromagnetic interactions in complex **2**.

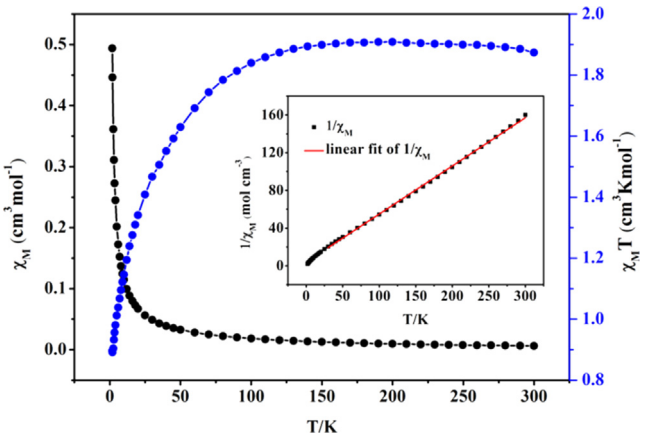

Fig. 4 The χ_M^{-1} and χ_MT versus T for complex **1**. (Insert the fits red line).

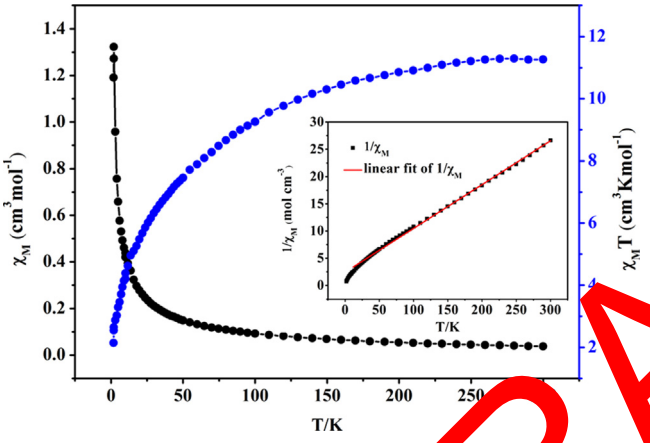

Fig. 5 The χ_M^{-1} and χ_MT versus T for **2**. (In[illegible] the [illegible]

3.3. Compound significantly reduced the A549 NSCLC cells viability

After synthesis of compounds **1** and **2**, their inhibitory activity against the NSCLC cancer cell viability were measured in this present research. The cell counting kit-8 was accomplished totally in accordance with the manufactures' instruction with some changes. As the results showed in Fig. 6, we can see that compared with the control group, compound **1** could significantly reduce the viability of the A549 NSCLC cells, while compound **2** showed almost no influence against the A549 NSCLC cells viability. In addition to this, all the metal ions and ligands of compound **1** or **2** exhibited no suppression on the viability of A549 NSCLC cancer cell. This result indicated that compound **1** was more effective than compound **2** in the PD-L1 treatment of NSCLC.

3.4. Compound obviously reduced the relative expression of ezh2 gene elative expression in the A549 NSCLC cells

ezh2 gene was usually high-expression in various cancer cells, which has been regarded as the indicator of cancer diagnosis.

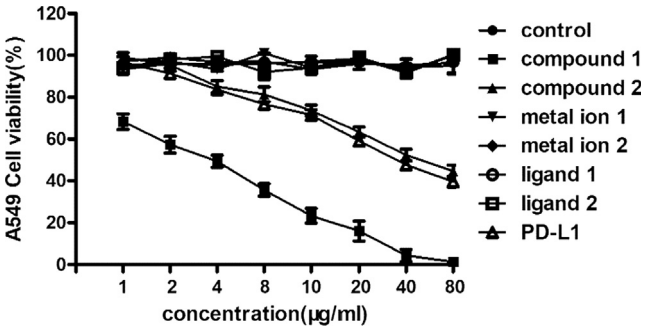

Fig. 6 Significantly reduced viability of the A549 NSCLC cells after treated with new compounds. The A549 NSCLC cells in logical growth phage were harvested and incubated into the 96 well plates, followed by compounds **1** and **2** treatment with serial diluted concentrations. The microplate reader was used to measure the absorbance of each wells at 480 nm. This experiment was repeated at least three times.

The inhibition of *ezh2* gene have achieved good efficacy in early clinical trials indicating that the ZH2 protein is a potential therapeutic target. So, the inhibitory activity of the new compounds on the *ezh2* gene expression in the A549 NSCLC cells was determined with real time RT-PCR. The results in Fig. 7 exhibited that there was a significantly increased level of the *ezh2* gene expression, which is obviously different from the normal lung cells. However, after compound **1** treatment, the expression levels of the *ezh2* gene was reduced significantly, which is much stronger than that of compound **2**. In addition to this, all the metal ions and ligands of compound **1** or **2** exhibited almost no influence on the *ezh2* gene expression.

4. Conclusion

To sum up, we have produced two new coordination polymers by employing 5-((4-carboxypyridin-2-yl)amino)isophthalic acid (H_3L), a semirigid carboxylate-pyridine ligand with V-shape. The as-synthesized two polymers were completely explored with PXRD, TGA, the diffraction of single crystal X-ray, IR spectroscopy as well as EA. Magnetic investigations have suggested that there is antiferromagnetic coupling between neighboring metal ions in the two compounds. The results of the CCK-8 assay indicated that compound **1** was more excellent than compound **2** on inhibiting the viability of the NSCLC cells. Besides, the data of the real time RT-PCR revealed that compound **1** could significantly inhibit the relative expression of the *ezh2* gene in the NSCLC cells, but compound **2** exhibited only a little change on the *ezh2* gene expression. In the end, we draw this conclusion, compound **1** was much more excellent than compound **2** on the NSCLC treatment, which could reduce the *ezh2* gene expression in A549 NSCLC cells and inhibiting cancer cell viability.

Data availability

The data used to support the findings of this study are included within the article.

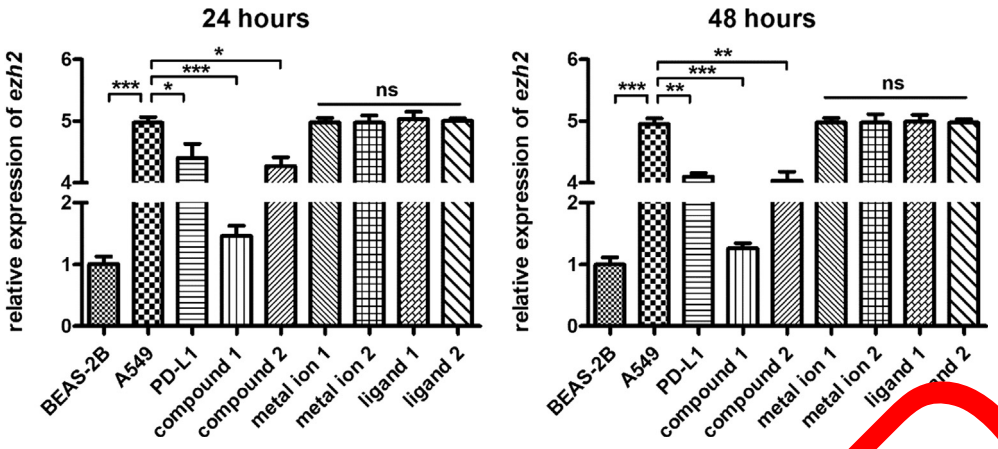

Fig. 7 Obviously reduced relative expression of *ezh2* gene elative expression in the A549 NSCLC cells after ated via co ounds **1** and **2**. The A549 NSCLC cells in logical growth phage were harvested and inoculated into the 96 well pl s, follow by com unds **1** and **2** treatment at indicated treatment. The real time reverse transcription polymerase chain reaction w s performed to te of the *ezh2* gene expression in A549 NSCLC cells.

Declaration of Competing Interest

The authors declare that they have no known competing financial interests or personal relationships that could have appeared to influence the work reported in this paper.

Acknowledgments

The research was supported by Natural Science Foundation o Jiangsu Province (BK20181175) and National Natural Scien Foundation of China (81972800).

Appendix A. Supplementary material

Supplementary data to this article ca be fo online at https://doi.org/10.1016/j.arabjc.2020 2921.

References

Bai, N., Gao, R., Wang, H. u, Y., H u, L., Wang, Y.Y., 2018. Five transition metal coor ation ymers driven by a semirigid trifunctional nicotinic ac id: selecti adsorption and magnetic properties EngC n 20, 57 –5734.

Chen, K.J., Ma en, D , Phal T orrest, K.A., Kumar, A., Yang, Q.Y Xue, W pace, B., Perry, J.J., Zhang, J.P., Chen, X. M., Zawo ko, M , Tuning pore size in square-lattice coordination orks for size-selective sieving of CO_2. Angew. Chem. Int. Ed. 10268–10272.

Coudert, F.X., Fuchs H., 2015. Computational characterization and prediction of metal-organic framework properties. Coord. Chem. Rev. 307, 211–236.

Cui, H.H., Lv, W., Tong, W., Chen, X.T., Xue, Z.L., 2019. Slow magnetic relaxation in a mononuclear five-coordinate Cu(II) Complex. Eur. J. Inorg. Chem. 43, 4653–4659.

de Sousa, V.M.L., Carvalho, L., 2018. Heterogeneity in lung cancer. Pathobiology 85, 96–107.

Duan, C., Dong, L., Li, F., Xie, Y., Huang, B., Wang, K., Yu, Y., Xi, H., 2020. Room-temperature rapid synthesis of two-dimensional metal-organic framework nanosheets with tunable hierarchical porosity for enhanced adsorption desulfurization performance. Ind. Eng. Chem. Res. 59, 18857–18864.

Han, Z., Yu, Y hang, Y., D B., ng, A., Shan, Y., 2015. Al-coordinati p mer-derived porous nitrogen-doped carbon microfibers as me free catalysts for oxygen electroreduction and acetalization reaction J. Mater. Chem. A 3, 23716–23724.

He, P., Yan, Y.X., Zh g, J., 2020. Functional metal–organic frameworks constructed from triphenylamine-based polycarboxylate ligands. C rd. Chem. Rev. 420, 213354.

Jia N., Liu, Y Yu, X.N., Zhang, H.B., Wang, M.M., 2020. C osion re tance of nickel-phosphorus/nano-ZnO composite multi coating electrodeposited on carbon steel in acidic chloride environments. Int. J. Electrochem. Sci. 15, 5520–5528.

Jarma , A., Desai, A.V., Ghosh, S.K., 2016. Ionic metal-organic frameworks (iMOFs): Design principles and applications. Coord. Chem. Rev. 307, 313–341.

Liu, B., Wei, L., Li, N.N., Wu, W.P., Miao, H., Wang, Y.Y., Shi, Q. Z., 2014. Solvent/temperature and dipyridyl ligands induced diverse coordination polymers based on 3-(2′,5′-dicarboxylphenyl)pyridine. Cryst. Growth Des. 14, 1110–1127.

Mao, Y., Yang, D., He, J., Krasna, M.J., 2016. Epidemiology of lung cancer. Surg. Oncol. Clin. N. Am. 25, 439–445.

Mukherjee, S., Ganguly, S., Manna, K., Mondal, S., Mahapatra, S., Das, D., 2018. Green approach to synthesize crystalline nanoscale Zn(II)-coordination polymers: cell growth inhibition and immunofluorescence study. Inorg. Chem. 57, 4050–4060.

Rancan, M., Armelao, L., 2015. Exploiting dimensional variability in coordination polymers: Solvent promotes reversible conversion between 3D and chiral 1D architectures. Chem. Commun. 51, 12947–12949.

Rodriguez-Canales, J., Parra-Cuentas, E., Wistuba, I.I., 2016. Diagnosis and molecular classification of lung cancer. Cancer Treat. Res. 170, 25–46.

Romaszko, A.M., Doboszyńska, A., 2018. Multiple primary lung cancer: A literature review. Adv. Clin. Exp. Med. 27, 725–730.

Sen, R., Halder, A., Ghoshal, D., 2020. Three mixed ligand coordination polymers: Syntheses, characterization and detailed study of the structural transformations. Polyhedron 183, 114534.

Yang, C.B., Jiang, C.B., Zhang, M.Y., Chen, X., Zou, P., Yang, R.W., Rao, H.B., Wang, G.T., 2020. A multifunctional Eu-based coordination polymer luminescent sensor for highly sensitive and selective detection of Fe^{3+} and acetone. Polyhedron 175, 114216.

Yang, E.C., Liu, Z.Y., Wu, X.Y., Chang, H., Wang, E.C., Zhao, X.J., 2011. Co(II), Mn(II) and Cu(II)-directed coordination polymers with mixed tetrazolate–dicarboxylate heterobridges exhibiting spin-canted, spin-frustrated antiferromagnetism and a slight spin-flop transition. Dalton Trans. 40, 10082–10089.

Yao, R.X., Qin, Y.L., Ji, F., Zhao, Y.F., Zhang, X.M., 2013. Triangle, square and delta-chain based cobalt tetrazolate magnets. Dalton Trans. 42, 6611–6618.

Zhang, Y.J., Yin, L., Li, J., Hu, Z.B., Ouyang, Z.W., Song, Y., Wang, Z., 2020. Synthesis, crystal structures, HF-EPR, and magnetic properties of six-coordinate transition metal (Co, Ni, and Cu) compounds with a 4-amino-1,2,4-triazole Schiff-base ligand. RSC Adv. 10, 12833–12840.

Zhao, Y., Dang, L.L., Zhai, Z.M., Ma, L.F., Wang, L.Y., 2020. Crystal structures and magnetic properties of two Co(II) coordination polymers created via in situ ligand synthesis. J. Solid State Chem. 290, 121573.

Zhao, J., Zhang, J., Zhang, D., Hu, Z., Sun, Y., 2021. Effect of emerging pollutant fluoxetine on the excess sludge anaerobic digestion. Sci. Total Environ. 752, 141932.

Zheng, L.N., Wei, F.H., Hu, H.M., Bai, C., Yang, X.L., Wang, X., Xue, G., 2019. Lanthanide coordination polymers constructed from the asymmetrical N-heterocyclic rigid carboxylate: Synthesis, crystal structures, luminescence properties and magnetic properties. Polyhedron 161, 47–55.